BNL-215885-2020-TECH

EIC-APG-TN-001

Limiting Coherent Longitudinal Beam Oscillations in the EIC Electron Storage Ring

B. Podobedov

April 2020

Electron-Ion Collider Project

Brookhaven National Laboratory

U.S. Department of Energy

USDOE Office of Science (SC), Nuclear Physics (NP) (SC-26)

Notice: This technical note has been authored by employees of Brookhaven Science Associates, LLC under Contract No.DE-SC0012704 with the U.S. Department of Energy. The publisher by accepting the technical note for publication acknowledges that the United States Government retains a non-exclusive, paid-up, irrevocable, world-wide license to publish or reproduce the published form of this technical note, or allow others to do so, for United States Government purposes.

DISCLAIMER

This report was prepared as an account of work sponsored by an agency of the United States Government. Neither the United States Government nor any agency thereof, nor any of their employees, nor any of their contractors, subcontractors, or their employees, makes any warranty, express or implied, or assumes any legal liability or responsibility for the accuracy, completeness, or any third party's use or the results of such use of any information, apparatus, product, or process disclosed, or represents that its use would not infringe privately owned rights. Reference herein to any specific commercial product, process, or service by trade name, trademark, manufacturer, or otherwise, does not necessarily constitute or imply its endorsement, recommendation, or favoring by the United States Government or any agency thereof or its contractors or subcontractors. The views and opinions of authors expressed herein do not necessarily state or reflect those of the United States Government or any agency thereof.

EIC TECHNICAL NOTE	NUMBER **EIC-APG-TN-001**
AUTHORS: Boris Podobedov & Michael Blaskiewicz	DATE April 28, 2020
Limiting Coherent Longitudinal Beam Oscillations in the EIC Electron Storage Ring	

1. Introduction

We study coherent longitudinal beam oscillations in the BNL EIC electron storage ring (ESR). This is motivated by two factors. First, the present ESR design is expected to have longitudinal coupled bunch instability, driven primarily by a narrow-band impedance due to the RF cavity HOM absorbers [1]. A strategy needs to be developed to cure this instability, either by passive damping with re-designed HOM absorbers, or by active means with a longitudinal feedback system. Second, as it will be shown in Section 2 below, to avoid unacceptable hadron emittance growth, the electron beam arrival time jitter in the crab cavities must be maintained below 1.1 ps rms, which imposes 0.33 mm rms limit on the amplitude of coherent longitudinal oscillations in the ESR. These oscillations are expected to be primarily driven by the RF phase noise. However, in the case that a feedback system is used to cure the instability, they can also come from the feedback system itself, which, in a certain frequency range, essentially amplifies its own sensor noise. In this note we will derive the expected magnitude of these oscillations for either approach, and recommend the one with the feedback system to be taken.

The rest of this note is organized as follows. In Section 2 we derive the limit for the longitudinal arrival time oscillation amplitude in the crab cavities. In Section 3 we work out the longitudinal oscillation amplitude in the presence of the instability and feedback using a model of noise-driven harmonic oscillator with a derivative controller. Section 4 discusses typical values for the RF phase noise and longitudinal bunch-by-bunch feedback sensor noise achieved at NSLS-II and elsewhere, which we argue could serve as a reference for the ESR design. Section 5 presents numerical estimates for the amplitude of longitudinal beam jitter in the EIC ESR with and without the feedback. Finally, in Section 6 we summarize our results.

2. Limit for longitudinal position oscillation amplitude in ESR

Longitudinal motion of the electron bunches creates dipole beam-beam kicks on the hadrons because of the crossing angle. This is reduced by the crab cavities but not removed. We begin by deriving the transverse kick from the electrons and then address emittance growth of the hadrons.

Let z denote the longitudinal position of an electron with respect to the zero crossing of the crab voltage with $z>0$ at the head of the bunch. As this particle moves through the interaction region its offset from the ideal orbit is

$$\Delta x(z) = \theta z - \theta \sin(kz)/k\,. \tag{2.1}$$

In equation (2.1) θ is the half crossing angle 12.5 mrad, and k =8.25 m^{-1} is the wavenumber of the crab cavity (corresponding to 394 MHz frequency [1]). Suppose the electron bunch centroid is oscillating as $z_0(t)$. Then, the average offset of the electron bunch is

$$\langle \Delta x(t) \rangle = \int ds \Delta x(s) f(s - z_0(t)). \tag{2.2}$$

In equation (2.2) $f(s)$ is the longitudinal distribution function of the electron bunch, which we model as a Gaussian of rms width σ_l. Expanding the sine to cubic order one gets

$$\langle \Delta x(t) \rangle = \theta k^2 < (s - z_0(t))^3 >_s /6 \cong -\theta k^2 \sigma_l^2 z_0(t)/2, \tag{2.3}$$

where we assume the average oscillation amplitude is zero and that the oscillation is small compared with the bunch length. This transverse offset creates a beam-beam dipole kick which can drive hadron emittance growth [2]. The hadron beam size at the interaction point grows as

$$\frac{d}{dn}\sigma_x^2 = 2(2\pi \Delta Q_{bb} \sigma_{xe})^2 \sum_{m=-\infty}^{\infty} \rho(m) \cos(2m\pi Q_x)\,. \tag{2.4}$$

In equation (2.4) n denotes turn number, σ_x is the horizontal beam size, ΔQ_{bb} is the beam-beam tune shift, σ_{xe} is the rms value of $\langle \Delta x \rangle$, $\rho(m)$ is its correlation function in turns, and Q_x is the horizontal tune.

Depending on the correlation function the sum can be very large, but since the synchrotron tune is smaller than the betatron tune, this is unlikely. As an initial estimate we take the sum to be 1. We take the initial beam size to be σ_{x0} =0.1 mm, ΔQ_{bb}=0.015, and n=10 hours/12.8 microseconds, for the beam emittance to double. This yields σ_{xe}=14 nm. Using equation (2.3) one gets an rms value of z_0 of 0.08 mm for σ_l=20 mm bunch length. If there is no third harmonic cavity the electron bunch length is about one centimeter and the rms value of z_0 is 0.33 mm, or, equivalently, the electron beam arrival time jitter in the crab cavities must be maintained below 1.1 ps rms.

3. Analytical model for longitudinal beam oscillations

In this section x stands for the coordinate of a general 1D harmonic oscillator. The results could be applied to storage ring beam dynamics in the transverse or the longitudinal plane. In Section 5 below we will apply them to the longitudinal motion in the ESR, making a replacement $x \to z$.

3.1. White noise driven harmonic oscillator with feedback

Consider a unit-mass, damped harmonic oscillator driven by white noise, which is controlled by derivative feedback,

$$\ddot{x} + 2\Gamma\dot{x} + \omega_0^2 x = \sigma\,\eta(t) - g \times (\dot{x} + \dot{\xi}(t)), \tag{3.1}$$

where ω_0 is the natural frequency, $\Gamma > 0$ is the damping decrement, $\sigma\,\eta(t)$ is a stochastic force with zero mean and δ-function autocorrelation, $R(\tau) = \sigma^2\delta(\tau)$, g and $\xi(t)$ are the feedback gain and sensor noise. If the drive noise, $\eta(t)$, and the sensor noise, $\xi(t)$, are uncorrelated, the expected power spectral density (PSD) of x is given by (i.e. [3]),

$$S_x(\omega) = \frac{\sigma^2}{(\omega_0^2-\omega^2)^2+(2\Gamma+g)^2\omega^2} + \frac{g^2\omega^2}{(\omega_0^2-\omega^2)^2+(2\Gamma+g)^2\omega^2}\sigma_\xi^2. \tag{3.2}$$

Here the sensor noise PSD is assumed constant in the frequency range of interest, $S_\xi(\omega) = S_\xi = \sigma_\xi^2$. Denoting the sensor noise bandwidth (in rad/s) by B_ξ, the total integrated sensor noise power (in m^2) is then

$$\sigma_s^2 = \frac{1}{2\pi}\int S_\xi(\omega)d\omega = \frac{B_\xi}{\pi}\sigma_\xi^2\ . \tag{3.3}$$

Integrating (3.2) over frequency, we get for the expected rms of the residual oscillation σ_x,

$$\sigma_x^2 = \frac{1}{2\pi}\int S_x(\omega)d\omega = \frac{{\sigma_{x0}}^2}{1+\frac{1}{2}g/\Gamma} + \frac{g^2\sigma_\xi^2}{2(2\Gamma+g)}, \tag{3.4}$$

where σ_{x0} denotes the expected rms of the residual oscillation without the feedback (at $g = 0$),

$$\sigma_{x0} = \sqrt{\langle x^2\rangle} = \frac{\sigma}{2\omega_0\sqrt{\Gamma}} = \frac{\omega_0}{2}\sqrt{\frac{S_x(0)}{\Gamma}}. \tag{3.5}$$

Combining (3.3) and (3.4), we obtain the fractional change in the power of the residual oscillations due to the feedback,

$$\frac{\sigma_x^2}{{\sigma_{x0}}^2} = \frac{1+\frac{\pi}{4}\frac{g^2}{\Gamma^2}\Gamma\sigma_s^2/B_\xi}{1+\frac{1}{2}g/\Gamma}\ . \tag{3.6}$$

As expected, increasing the feedback gain from zero results in the initial reduction of the residual oscillation power. When the second term in the numerator of (3.6) takes over, the residual oscillations start to increase, eventually exceeding the level without the feedback. For a noiseless sensor the model results in infinitely small residual oscillations in the limit of infinitely large feedback gain.

From (3.6) it is easy to find the optimal feedback gain which minimizes the residual oscillation for a given sensor noise level,

$$g_{opt} = 2\Gamma\left(\sqrt{1+\alpha^2}/\alpha - 1\right), \tag{3.7}$$

where we introduced parameter α to express the normalized sensor noise amplitude,

$$\alpha = \sqrt{\frac{\pi\Gamma}{B_\xi}}\frac{\sigma_s}{\sigma_{x0}} = \frac{2\Gamma}{\omega_0}\sqrt{\frac{S_\xi}{S_x(0)}}\,. \tag{3.8}$$

Note that for all practical situations $\Gamma \ll \omega_0$, so, for any reasonably good feedback sensor, this parameter is expected to be small, $\alpha \ll 1$.

Finally, the minimum level of the residual oscillations at the optimum feedback gain is given by

$$\frac{{\sigma_{x,min}}^2}{{\sigma_{x0}}^2} = 2\alpha\left(\sqrt{1+\alpha^2} - \alpha\right), \tag{3.9}$$

therefore, in the limit of small sensor noise, the residual oscillations will be substantially reduced by the feedback,

$$\sigma_{x,min} = \sigma_{x0}\sqrt{2\alpha}, \quad \alpha \ll 1\,. \tag{3.10}$$

Fig. 1 illustrates this in the frequency domain. Note that at every sensor noise level there is some increase in the high-frequency PSD compared to the no-feedback case, however the integrated power is always lower with the feedback, in agreement with (3.9).

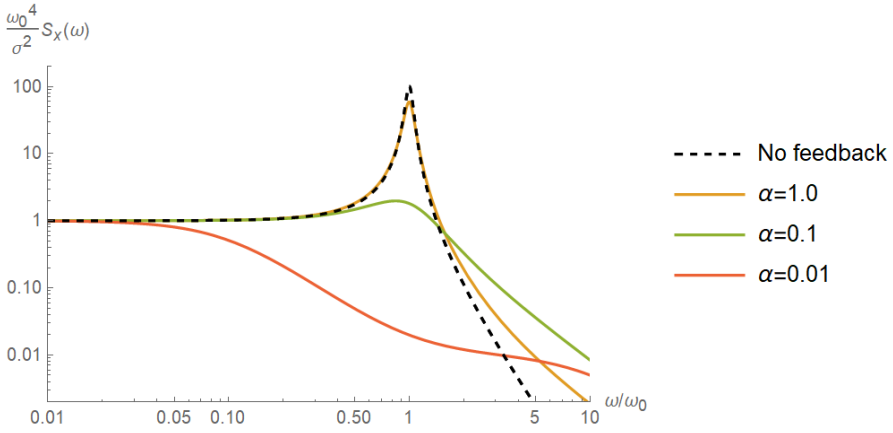


Figure 1: PSD of residual oscillations at the optimum feedback gain plotted for different feedback sensor noise levels and $\Gamma/\omega_0 = 0.05$.

3.2. Adding the instability

So far we considered a stable situation, $\Gamma > 0$, and showed that the optimized derivative feedback with a low-noise sensor can substantially reduce the residual noise due to a stochastic driving force.

In the context of electron storage ring longitudinal beam dynamics (well described by a damped harmonic oscillator model, see i.e. [4]) this applies to the common case of longitudinally stable beam, driven by RF noise (primarily m=0 mode). It is well-known that a bunch-by-bunch feedback system, which essentially acts on all coupled-bunch modes, can effectively reduce the residual beam noise in this case. In practice, feedback controllers for such systems utilize a band-limited differentiator implemented as a digital FIR filter [5], i.e. they are more complicated than a simple

derivative controller used in our model. Nevertheless, we believe that our controller model is appropriate for the preliminary design estimates to be worked out in this note.

Now we are extending the model to estimate how the feedback will affect the residual beam noise, when, in addition to the white noise drive considered so far, there is an instability the feedback needs to damp.

To include beam instability, we need to:

1) replace, $\Gamma \to \Gamma_d - \Gamma_i$, in (3.1), where Γ_d is the radiation damping rate, assumed fixed, and $\Gamma_i > 0$ is the instability growth rate,

$$\ddot{x} + 2(\Gamma_d - \Gamma_i)\dot{x} + \omega_0^2 x = \sigma\,\eta(t) - g \times (\dot{x} + \dot{\xi}(t)); \tag{3.11}$$

2) Proceed as above, except only consider the feedback gains such that, $\Gamma_d - \Gamma_i + g > 0$, so that the beam is stable with feedback;

3) Normalize the residual motion rms to that for the case without the feedback and instability, i.e. replace, $\Gamma \to \Gamma_d$, in (3.5) to obtain

$$\sigma_{x0} = \frac{\sigma}{2\omega_0\sqrt{\Gamma_d}} = \frac{\omega_0}{2}\sqrt{\frac{S_x(0)}{\Gamma_d}}\,. \tag{3.12}$$

The equivalent of (3.6) becomes

$$\frac{\sigma_x^2}{{\sigma_{x0}}^2} = \frac{1}{1+\frac{1}{2}(g-2\Gamma_i)/\Gamma_d}\left(1 + \frac{\pi}{4}\,\frac{g^2}{\Gamma_d B_\xi}\,\frac{\sigma_s^2}{{\sigma_{x0}}^2}\right). \tag{3.13}$$

Similarly to Section 3, finding the optimum feedback gain is equivalent to minimizing the function

$$f(y) = \frac{1+\alpha^2 y^2}{1+y-y_i}, \tag{3.14}$$

where $\mathrm{y} = \frac{1}{2}g/\Gamma_d$, $\mathrm{y}_i = \Gamma_i/\Gamma_d$, and the sensor noise parameter α is given by

$$\alpha = \sqrt{\frac{\pi\Gamma_d}{B_\xi}}\,\frac{\sigma_s}{\sigma_{x0}} = \frac{2\Gamma_d}{\omega_0}\sqrt{\frac{S_\xi}{S_x(0)}}\,. \tag{3.15}$$

The minimum level of the residual oscillations occurs for the optimum feedback gain of

$$g_{opt} = 2\Gamma_d\left(\sqrt{1+\alpha^2(\Gamma_i/\Gamma_d - 1)^2}/\alpha + \Gamma_i/\Gamma_d - 1\right), \tag{3.16}$$

and is given by

$$\frac{{\sigma_{x,min}}^2}{{\sigma_{x0}}^2} = 2\alpha\left(\sqrt{1+\alpha^2(\Gamma_i/\Gamma_d - 1)^2} + \alpha(\Gamma_i/\Gamma_d - 1)\right). \tag{3.17}$$

As expected, these two equations are identical to (3.7) and (3.9) for $\Gamma_i = 0$.

Consider α<<1 regime, which we argued before is the usual situation in the longitudinal plane. Here the asymptotics of (3.17) for small and large values of Γ_i/Γ_d parameter become 2α and $4\alpha^2\Gamma_i/\Gamma_d$ respectively. They intersect at $\Gamma_i/\Gamma_d = \frac{1}{2\alpha}$. Therefore, as long as the instability growth rate is lower than this value,

$$\frac{\Gamma_i}{\Gamma_d} < \frac{1}{2\alpha}, \tag{3.18}$$

the feedback is very effective, and it reduces beam oscillation power by a large factor,

$$\frac{{\sigma_{x,min}}^2}{{\sigma_{x0}}^2} = 2\alpha, \ \alpha \ll 1. \tag{3.19}$$

The reduction (or increase) of the residual beam oscillation power due to the feedback in the presence of instability, described by (3.17), is illustrated in Fig. 2, as a function of the instability growth rate. It shows that the feedback is ineffective when the sensor noise is large. It also shows that for any instability growth rate one could peak a feedback sensor with low enough noise (given by (3.18)) that the feedback will reduce the residual oscillations by a large factor given by (3.19).

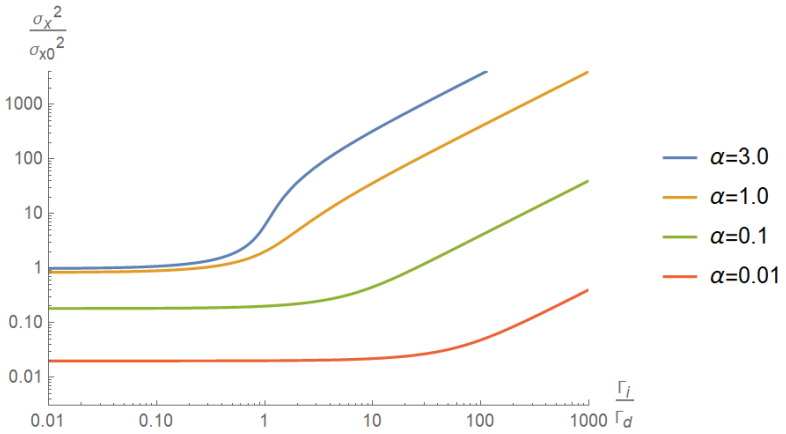


Figure 2: Residual oscillation power with the derivative feedback set to the optimum gain plotted for different feedback sensor noise levels.

In Fig. 2 we normalize the oscillation power to that without the instability and feedback, (3.12), which in turn depends on the magnitude of the drive noise. For a storage ring application, the latter is primarily given by the RF phase noise, which has not been specified yet for the ESR RF system design. To proceed further and estimate the magnitude of the electron beam oscillation in millimeters, we need to come up with a reasonable specification for the RF phase noise, as well as to estimate if the required feedback sensor noise performance is realistic. First, to get a feel for these parameters, we present some examples from the NSLS-II storage ring light source at BNL.

4. Typical values for RF phase noise and longitudinal BPM noise demonstrated at NSLS-II

In modern synchrotron light sources the most stringent limit for the magnitude of beam oscillations in the longitudinal plane usually comes from the timing users. For instance, in the NSLS-II PDR [6] the required beam motion below 5% of rms bunch length (assumed 10 ps in the PDR), required by the timing experiments, specifies the tightest requirement for the RF phase jitter equal to 0.16 degree of RF phase ($f_{RF} = 500$ MHz). This specification has been achieved by a large margin.

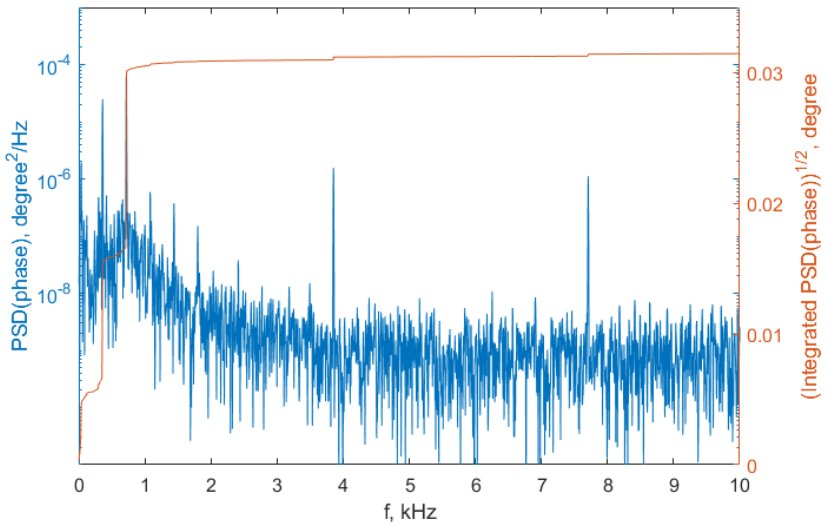


Figure 3: RF cavity phase noise from 0.2 sec time-domain buffer sampled at 4 MHz. The cavity is set to the nominal operating voltage of 1.5 MV.

To illustrate this, Fig. 3 presents the phase noise measurement for one (of the two total) NSLS-II RF cavities set to the nominal voltage of 1.5 MV, with 2 mA of beam current in the ring (this low-current beam does not affect the measurement). The integrated noise is about 0.03 degree rms in 10 kHz bandwidth. Apart from low-frequency broad-band contribution, the noise includes power-line harmonics (i.e. 360 Hz, 720 Hz, etc.), as well as subharmonics of the solid-state pulse switch modulated high voltage power supply, powering the klystron (3.85 kHz and 7.7 kHz lines in the plot).

Cavity probe signals, used for the measurement shown in Fig. 3, are routinely monitored during high current beam operations, in which case the measured phase noise also includes a substantial contribution from the electron beam. Typical integrated phase noise at 400 mA measures 0.1-0.2 degree rms in 2 MHz bandwidth, and less than 0.05 degree rms in 10 kHz bandwidth. For reference, NSLS-II revolution frequency is 3.78 kHz and the synchrotron frequency at high current is ~2 kHz.

Similarly, 0.1-0.2 degree rms RF phase noise values have been reported by several other light sources, all with the main RF frequency in the usual range of 350 to 500 MHz.

With regards to the longitudinal feedback system sensor (BPM) noise performance, we again present an example from NSLS-II. Even though the coupled-bunch motion at NSLS-II is stable at full design current of 0.5 A, the light source is equipped with a longitudinal bunch-by-bunch (BxB) system front-end from Dimtel for monitoring and diagnostic purposes. (On top of that, NSLS-II has two complete BxB feedback systems for both transverse planes, which are required to damp the respective instabilities during operations).

Fig. 4 shows typical signals from the longitudinal BxB system front-end during 400 mA current, presently used in routine operations. The first 1200 RF buckets (out of 1320 total) are filled approximately uniformly, and a single "camshaft" bunch is added to the bucket 1281.

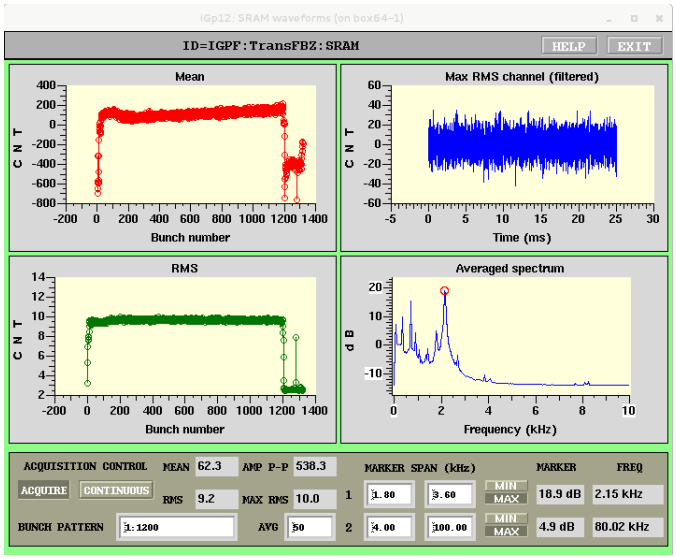


Figure 4: Longitudinal BxB feedback front-end signals at 400 mA. Fill pattern consists of 1200-bunch uniform train plus a camshaft bunch at bucket 1281.

The two plots relevant to this technical note are at the bottom. The left shows the longitudinal oscillation rms for each bunch, while the right plot shows the spectral content of these oscillations, averaged over the bunch train. As expected, the longitudinal beam motion occurs dominantly near the synchrotron frequency (here f_s=2.2 kHz), as well as at lower frequencies, where distinct peaks due to power-line harmonics, i.e. 720 Hz, are clearly visible. There is virtually no motion at frequencies above $2f_s$. From the left plot, buckets 1-1200 measure ~9.8 ADC counts rms motion, while the empty buckets (>1200, excluding the camshaft bunch) measure ~2.6 counts.

Using the calibration of 91 ADC counts per mA, per degree RF at 25 dB of front-end attenuation obtained during the system commissioning in 2014 [7-8], we can convert the displayed data (0.33 mA/bunch, 0 dB attenuation) to the degrees of RF phase. The result is 0.02-degree rms beam jitter for the filled buckets, and 0.005 degree rms jitter for the empty buckets. The last number is a good measure for the feedback BPM noise level. Clearly, this level is very small to affect the real beam jitter measurement at high current.

5. Beam arrival position jitter estimates for the EIC ESR

In this section we present numerical estimates for the amplitude of longitudinal oscillations in the EIC ESR with and without the longitudinal feedback, and work out some constraints on the magnitude of RF phase noise in both cases. Because we only consider longitudinal dynamics here, we will be making the replacement $x \to z$, in the relevant formulas derived in Section 3.

We take relevant parameters from the EIC PCDR [1], specifically the longitudinal radiation damping time (at 10 GeV), $\tau_d = 2000$ turns, corresponding the damping rate $\Gamma_d = 1/2000$ turns^{-1}, the instability growth rate $\Gamma_i = 2\pi/1000$ turns^{-1}, the synchrotron tune $\nu_s = \omega_s/\omega_{rev} = 0.05$, and the RF frequency $f_{RF} = 591$ MHz.

First consider the case without the instability, so that the beam oscillations are driven by the RF phase noise only. As is clear from (3.2), the beam response is resonantly enhanced around the synchrotron frequency and then is sharply falling off at higher frequencies (see the dashed curve in Fig. 1). Higher frequency RF noise is therefore largely irrelevant, so we limit our consideration to the noise centered around the synchrotron frequency, with a similar magnitude bandwidth, $B_{RF} \sim \omega_s$.

Let us assume that the phase noise of rms σ_ϕ (in degrees) is distributed uniformly in this bandwidth. The PSD of this noise, PSD_{RF}, can be expressed as

$$\frac{1}{\pi}\int_{\omega_s-\frac{1}{2}B_{RF}}^{\omega_s+\frac{1}{2}B_{RF}} PSD_{RF}\,d\omega = \frac{B_{RF}}{\pi} PSD_{RF} = {\sigma_\phi}^2, \text{ or} \tag{5.1}$$

$$PSD_{RF} = \frac{\pi}{B_{RF}}{\sigma_\phi}^2. \tag{5.2}$$

At low frequency the beam simply follows the RF, so, from Section 3 (where $S_x(\omega)$ stands for the oscillator motion PSD in units of meter^2×second/rad) we have, for the beam motion PSD,

$$S_z(0) = PSD_{RF}\left(\frac{c}{f_{RF}\,360}\right)^2 = \frac{\pi}{B_{RF}}\left(\frac{c}{f_{RF}\,360}\right)^2 {\sigma_\phi}^2. \tag{5.3}$$

The ratio in parenthesis is simply the degree of RF phase to position conversion factor. For 591 MHz frequency, 1 degree of RF phase corresponds to 1.41 mm.

Substituting (5.3) into (3.12), we obtain the final expression for the residual beam oscillation rms,

$$\sigma_{z0} = \sigma_\phi \frac{c}{f_{RF}\,360}\frac{1}{4}\sqrt{\frac{\pi B_{RF}}{\Gamma_d}}. \tag{5.4}$$

Plugging in the PCDR values, and taking, for instance, $\sigma_\phi = 0.1$ degree and $B_{RF} = \omega_s$, we obtain

$$\sigma_{z0} = \text{ 1.6 mm}, \tag{5.5}$$

which significantly exceeds the 0.33 mm rms crab cavity limit worked out in Section 2.

In order for the beam oscillation amplitude to end up right at this limit, we must reduce the RF phase noise proportionally, to about 0.02 degrees rms, which could be somewhat challenging in practice. On top of that, due to numerous approximations made, it would be prudent to assume a safety factor of 2-5 at this stage of the design. This however will easily bring the required RF phase noise spec beyond the state-of-the-art.

We now turn to the case of longitudinal instability being cured by the feedback. As discussed above, on top of curing the instability, the feedback can bring the residual beam oscillations down by a large factor, as long as the feedback BPM has a good signal-to-noise ratio. In dimensionless form this was described by (3.17). To illustrate the required sensor noise performance in real units, we can express (3.17) in terms of the integrated sensor noise, σ_s, by substituting the unitless noise parameter α from (3.15), resulting in

$$\sigma_{z,min}{}^2 = 2\sigma_{z0}{}^2 \sqrt{\frac{\pi\Gamma_d}{B_\xi}}\frac{\sigma_s}{\sigma_{z0}}\left(\sqrt{1+\frac{\pi\Gamma_d}{B_\xi}\left(\frac{\sigma_s}{\sigma_{z0}}\right)^2(\Gamma_i/\Gamma_d-1)^2}+\sqrt{\frac{\pi\Gamma_d}{B_\xi}}\frac{\sigma_s}{\sigma_{z0}}(\Gamma_i/\Gamma_d-1)\right), \qquad (5.6)$$

where the residual oscillation rms without the feedback is given by (5.4).

Assuming the PCDR parameters, in particular $\Gamma_i/\Gamma_d = 4\pi$, and setting the sensor bandwidth in (5.6) to one synchrotron frequency, $B_\xi = \omega_s$, we obtain the final result shown in Fig. 5. It plots the beam arrival position jitter vs. the feedback sensor noise for representative levels of RF phase noise.

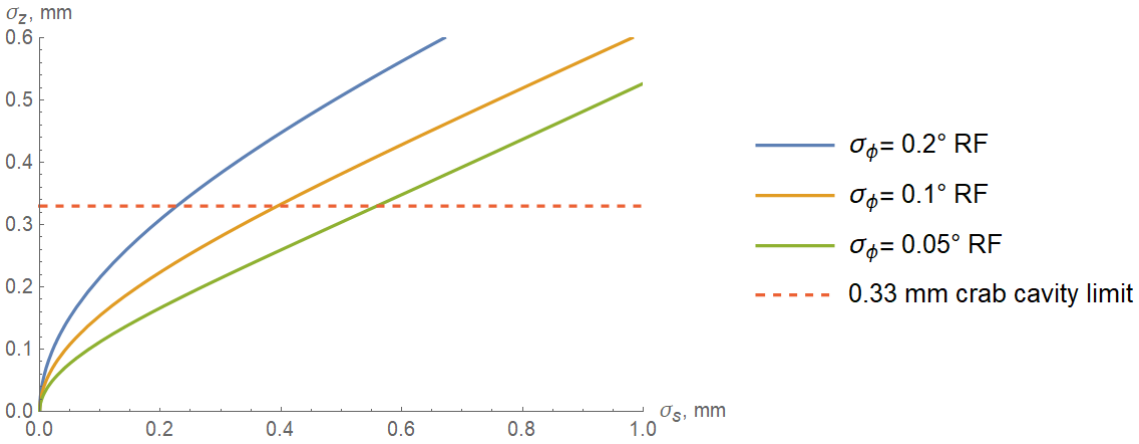


Figure 5: Beam arrival position jitter vs. integrated feedback sensor noise for several rms values of RF phase noise, σ_ϕ. Bandwidth of [0.5 1.5]ω_s is assumed for both the RF and sensor noise.

It illustrates that, for instance, for the RF noise level of σ_ϕ=0.1 degree rms, the sensor noise of 0.11 mm rms (or 0.078 degrees of RF phase), should be sufficient to maintain the beam arrival position jitter less than a factor of two of the 0.33 mm rms crab cavity limit derived in Section 2. This sensor noise level is a factor of 16 higher than what is measured at NSLS-II, and therefore we consider it readily achievable. Separately, bunch-by-bunch feedback BPM noise levels similar or better than at NSLS-II have been

demonstrated elsewhere [8]. In case more stringent RF phase jitter specs can be achieved in the ESR, the requirement for the feedback sensor noise performance will be even more relaxed.

6. Summary and outlook

To avoid unacceptable hadron emittance blow-up, the electron bunch arrival position jitter in the crab cavities must be maintained below 0.33 mm rms. This specification can be met in the presence of longitudinal coupled bunch instability by using a feedback damper. Our analysis predicts fairly relaxed specs for the RF phase noise (achieved at NSLS-II and elsewhere) as well as for the maximum allowable feedback sensor noise (also achieved). In addition to damping the unstable mode(s) the feedback will greatly reduce the amplitude of the (stable) m=0 mode that usually dominates the noise in the longitudinal plane.

An alternative option is to passively damp the instability (through the cavity damper redesign) but this will also require meeting much more challenging RF phase noise specs. This option is a seemingly inferior one.

Things could become more complicated with harmonic RF (not considered so far) which may require a further look. Modelling relevant effects in more detail can be done with Elegant and Matlab to help further specify relevant ESR systems.

7. References

[1] Electron-Ion Collider eRHIC Pre-Conceptual Design Report, BNL 205809-2018-FORE, v14, July 11, 2019

[2] M. Blaskiewicz, “Beam-Beam Damping of the Ion Instability”, NAPAC’2019, TUPLM11

[3] G.P. Conangla, Phys. Rev. Letters 122, 223602 (2019), DOI: 10.1103/PhysRevLett.122.223602

[4] S. Y. Lee, Accelerator Physics, 3rd Edition, World Scientific, 2011, https://doi.org/10.1142/8335

[5] D. Teytelman in Synchrotron Light Sources and Free-Electron Lasers, E.J. Jaeschke et al. (eds.), Springer, DOI 10.1007/978-3-319-14394-1_20, 2016

[6] NSLS-II Preliminary Design Report, BNL-94744-2007, 2007, https://www.bnl.gov/isd/documents/75003.pdf

[7] W. Cheng et al., “Commissioning of Bunch-by-bunch Feedback System for NSLS2 Storage Ring”, IBIC’2014, WEPD27

[8] Dmitry Teytelman, Private Communication, 2020